

The Vortex Glass-Liquid Transition in Fe_{1.02}Se Crystal

Elena Nazarova^{1,*}, Krastyo Buchkov¹, Armando Galluzzi², Konstantin Nenkov³,
Massimiliano Polichetti², Gunter Fuchs³

¹*G. Nadjakov Institute of Solid State Physics, Bulgarian Academy of Sciences, 72 Tzarigradsko Chaussee Blvd., Sofia, 1784, Bulgaria*

²*Department of Physics "E.R. Caianiello", University of Salerno, Giovanni Paolo II, 132, Salerno, I-84084, Italy & CNR-SPIN, C/o Giovanni Paolo II, 132, I-84084 Fisciano (SA), Italy*

³*Leibniz Institute for Solid State and Materials Research, Helmholtz str.20, Dresden, D-01171, Germany*

*Corresponding author: E-mail: nazarova@issp.bas.bg; Tel: (+359) 2 979 5679

Received: 24 February 2019, Revised: 08 May 2019 and Accepted: 14 May 2019

DOI: 10.5185/amlett.2019.0010

www.vbripress.com/aml

Abstract

The vortex-glass (VG) to vortex-liquid (VL) transition is studied in flux-grown Fe_{1.02}Se crystal with nanosized hexagonal phase inclusions. These non-superconducting impurities effectively pin the vortices and shift lightly the irreversibility line to higher fields and temperatures in comparison with single crystal. It is shown that the interplay between vortex pinning and thermal fluctuations enable the observation of VG-VL transition. The existence of this transition was proved by the scaling presentation of current-voltage characteristics at two different magnetic fields. The obtained scaling parameters are practically field independent. The values of the dynamic ν exponent are in the range predicted by the VG model, while the values of static ν exponent are a little smaller. This is not considered as a lack of the universality of the model, but rather as a consequence of the type of pinning and special domain morphology of the crystal resembling the granularity in polycrystalline samples. Copyright © VBRI Press.

Keywords: Superconductor, FeSe, vortex-glas to vortex-liquid transition.

Introduction

Superconductors are a special group of materials with unique electric and magnetic properties, specific functions and various applications. Up to now 32 classes of organic and inorganic superconducting compounds (including more than 1000 alloys, intermetallic compounds, ceramics, magnesium diboride, heavy fermions, iron-based superconductors etc.) are known [1]. The superconducting mechanism in conventional low- T_c superconductors is described by the Bardeen-Cooper-Schrieffer (BCS) theory based on electron - phonon interactions. The H-T phase diagram of these superconductors is very close to that predicted by the mean -field theory. The vortex-lattice melting coincides with the upper critical field $H_{c2}(T)$ line and practically there is no observable temperature range below $H_{c2}(T)$ with vortex-liquid (VL) phase (except for temperatures very close to T_c). Superconductors with properties not explained by the conventional theory because of their high critical temperature or other reasons suggesting different mechanism, form the group of the unconventional superconductors. Among them the most investigated are electron- and hole-doped cuprates and iron-based superconductors:

pnictides and chalcogenides, discovered ten years ago. In high- T_c superconductors, due to their specific characteristics (high T_c , small coherence length - ξ , large penetration depth - λ , large anisotropy) thermal (dynamic) and quenched (static) disorder significantly influence the vortex phase diagram and phase transitions. In the vortex matter the most obvious type of disorder is introduced by thermal fluctuations. Thermally activated jumps of the vortices described by the Anderson creep model, predict a resistivity state and reestablish the dissipation in the entire mixed state. Quenched disorder, when present in the samples, destroys the long-range order in the vortex lattice changing it in an arrangement determined by the randomly distributed pinning centers [2]. This vortex-glass (VG) state, similar to the magnetic order of spin glasses, is a real superconducting state with long range phase coherence and strictly zero resistivity in contrast to the flux creep model [3]. Different types of static disorder results in different types of vortex phase transitions [4]. Parallel columnar defects cause a Bose-glass to superfluid transition in the vortex matter. The intrinsic planar structure in high- T_c superconductors in magnetic field directed parallel to the CuO₂ layers leads

to a “smectic-crystal”- vortex-liquid transition. In the presence of random point defects, a vortex-glass to vortex-liquid phase transition was predicted to occur in the vortex matter [2, 3, 5-7] etc. In this framework, transport measurements bring up significant information in the process of studying the magnetic properties and phase transitions in the vortex matter [7].

In this article it is shown that the necessary conditions (pinning centers and thermal fluctuations) for the VG - VL phase transition observation are satisfied in the investigated $\text{Fe}_{1.02}\text{Se}$ crystal. Nano-sized inclusions from the non-superconducting hexagonal phase obtained during synthesis are effective pinning centers, improve the irreversibility line and application potential. In spite of the low T_c of this superconductor thermal fluctuations play a considerable role. The VG - VL transition is confirmed by scaling of current-voltage, V-I, characteristics. The demonstrated scaling behavior extends the universality of the predicted VG theory to the binary chalcogenide system and shows the similarity of vortex matter behavior of $\text{Fe}_{1.02}\text{Se}$ with that in other iron-based superconductors and cuprates.

Experimental

The $\text{Fe}_{1.02}\text{Se}$ crystals were grown using a NaCl/KCl flux technique from pre-sintered powders mixed in the indicated nominal composition. All procedures (weighing, grinding, pressing) were carried out in an argon filled glove box. The synthesis was performed in evacuated (10^{-3} Torr) and sealed quartz ampoules. More details of the crystals synthesis can be found elsewhere [8].

The crystal structure of the obtained samples was determined by XRD analysis using a Bruker D8 Advance diffractometer with Cu $K\alpha$ radiation ($\lambda = 1.54056 \text{ \AA}$) and a LynxEye detector. The phase identification was performed with the Diffrac-plus EVA using an ICDD-PDF2 Database. The samples' morphology is characterized by a dual-beam scanning electron focused ion beam system (SEM/FIB LYRA I XMU, TESCAN), equipped with an EDX detector (Quantax 200, Bruker).

The transport measurements V(I) characteristics at different temperatures and R(T) dependencies at different magnetic fields) were performed using the Quantum Design 14T PPMS. The standard four-point geometry was used (Fig. 1a). In order to minimize the Joule heating effect, the DC current was applied for a very short period of 0.002 sec. The voltage signal was detected within an error margin of several nano-volts. The magnetic field was applied perpendicular to the current direction in the (101) plane of the sample (Fig. 1b). The sample's cross section is approximately $S=0.229 \times 0.02 \text{ cm}^2 = 0.00458 \text{ cm}^2$ and the distance between the voltage contact pads is $L=0.098 \text{ cm}$. The electric field (E), current density (J) and resistivity (ρ) have been determined from the basic relations: $E=V/L$; $J=I/S$ and $\rho=E/J$.

Results and discussion

The primary reflexes in the X-ray diffractogram of the $\text{Fe}_{1.02}\text{Se}$ crystal indicate the presence of two phases. To identify them, additional investigations on a small piece of powdered crystal were performed. It was found that the main phase is a tetragonal one, P4/nmm, and its content is $\sim 82\%$. The detected impurity phase is a hexagonal one, its quantity is about 18% with an average grain size of crystallites of $\sim 46 \text{ nm}$. The coexistence of two crystallographically different phases presumes a complex crystal morphology described as an aggregate of domains. However, it is well known that in cuprate superconductors nano-sized particles from various phases (Y-211, La-211, CeO_2) could serve as effective pinning centers and enhance the critical current. In our case, the nano-sized non-superconducting inclusions naturally obtained during the preparation process of the investigated crystal are expected to pin efficiently the vortices in the mixed state.

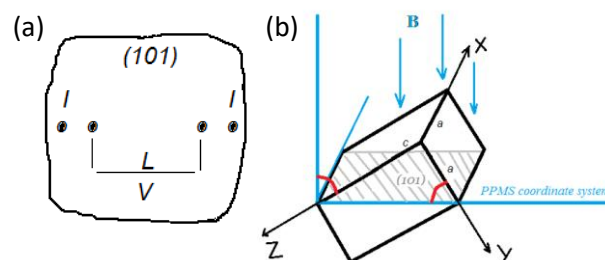


Fig. 1. (a) Four-point contact scheme. (b) Sample's unit cell in the measurement (PPMS) coordinate system.

In Fig. 2a, the $\rho(T)$ dependencies are presented for several magnetic fields in the range of 0-14T. From these curves the critical temperature $T_c(\rho=0)$ and the superconducting transition width ($10\% - 90\% \rho_n$) are determined, where ρ_n is the normal state resistivity (Fig. 2a). For increasing magnetic field, the $\rho(T)$ curves shift to lower temperatures, and a broadening of the superconducting transition (from $\Delta T=1.77 \text{ K}$ to $\Delta T = 2.58 \text{ K}$, respectively) is observed. The enhanced $T_c \sim 10.6 \text{ K}$ of the crystal, compared to $T_c \sim 8.1 \text{ K}$ for a single phase FeSe crystal, is explained by the internal stress due to the presence of the impurity hexagonal phase. The increased transition width is usually accepted as an indication of thermally activated flux dynamic. A weak magnetoresistive (MR) effect is observed, when the magnetic field is increased from zero to 14 T. According to the relation: $MR = [R(H,T) - R_0(H=0,T)] / R_0(H=0,T)$, the MR effect is estimated to be $\sim 11\%$ at $T=15 \text{ K}$. A MR effect was reported in compensated semimetals [9] and in high-quality FeSe and $\text{FeSe}_{1-x}\text{S}_x$ single crystals obtained by the vapor transport method [10]. This MR effect is closely related to the multi-band structure of the FeSe compound. FeSe is a compensated semimetal with two types of carriers: electrons and holes [11, 12]. In such materials, the MR effect is expected. The well-known structural transition determined in high-quality single

crystals at $T_s \sim 86$ K [10] and a nematic state established at $T < T_s$ change dramatically the band structure and the properties of FeSe [13, 14]. In this context, T_s is an important characteristic and its determination is essential. It has been found that in FeSe_{1-x}S_x single crystals T_s decreases to 49 K due to the chemical pressure caused by partial isovalent substitution of Se by S [10]. The $R(T)$ dependence at $H = 0$ and its derivative $d\rho/dT$ are presented in the Fig. 2b. The anticipated structural transition in the investigated crystal occurs at $T_s \sim 60$ K. By analogy this low T_s value could be related to internal pressure resulting from the presence of the hexagonal impurity phase.

The magnetic field dependence of the pinning activation energy $U(H)$ was determined as well. In the thermally activated flux flow regime (TAFF) and in the low current density limit the resistance is given by the relation: $R(H, T) = R_0 \exp(-U(H, T)/kBT)$, where k_B is the Boltzmann constant [15, 16]. The experimental data for $R(T)$ at different magnetic fields are presented in the Arrhenius plot, i.e. $\ln R$ plotted as a function of $1/T$. The pinning activation energy is determined from the slope of the linear part of the curves for the given magnetic field. The obtained result for the $U(H)$ dependence is presented in the Fig. 2c. The magnetic field dependence of the pinning activation energy is described by the relation: $U(H) \propto H^{-\alpha}$ with a crossover field $H_{cr} = 2.5$ T from single-vortex pinning regime to the collective-pinning regime. Pinning investigations of another crystal from the same batch revealed the presence of bulk pinning also [17]. The $U(H)$ dependence showing a similar trend, yields a crossover field $H_{cr} = 2.8$ T. The strength of the pinning force density is defined by the ratio J_c/J_0 , where J_c is the depinning critical current and J_0 is the depairing critical current [18]. Using the Bean critical state model, we established that J_c is in the order of 10^4 A/cm² (10^8 A/m²) at temperatures below 6 K [19] for these crystals. Based on experimental results for FeSe [20] the J_0 value is accepted to be $\sim 10^{11}$ A/m². Thus, for the dimensionless ratio J_c/J_0 we obtain the value $\sim 10^{-3}$ which is similar to the results obtained for YBCO superconductors ($10^{-3} - 10^{-2}$) [18]. This supports the assumption for the presence of weak pinning in these crystals, which is an important condition for the formation of disorder in the vortex matter.

Using the 10% and 90% ρ_n criterion, the irreversibility field $H_{irr}(T/T_c)$ and upper critical field $H_{c2}(T/T_c)$ lines are obtained, respectively, and presented in Fig. 2d. The $H_{irr}(T)$ line determines the region of application, limiting the applied magnetic field at which the material can sustain its supercurrent, while $H_{c2}(0)$ gives information on the pair-breaking mechanisms in magnetic field, the coherence length and anisotropic parameter. A very small anisotropy is characteristic for our samples even at temperatures close to T_c [17]. Large values of the Ginzburg-Landau parameter $\kappa \sim 72$ are obtained for FeSe, [21] which further increase to $\kappa \sim 104$ in Ag doped FeSe. [20]. For comparison, the $H_{irr}(T/T_c)$ and $H_{c2}(T/T_c)$ line for a single-phase FeSe single crystal [21] are presented in Fig. 2d as well. The

$H_{irr}(T/T_c)$ line for the investigated sample is lightly shifted to higher temperatures (especially for high fields) compared to the $H_{irr}(T/T_c)$ line of the single crystal. This is another indication for the presence of effective pinning in the investigated FeSe crystal. In such strong type-II superconductors with effective pinning centers, a rich vortex phase diagram and phase transitions are expected to exist.

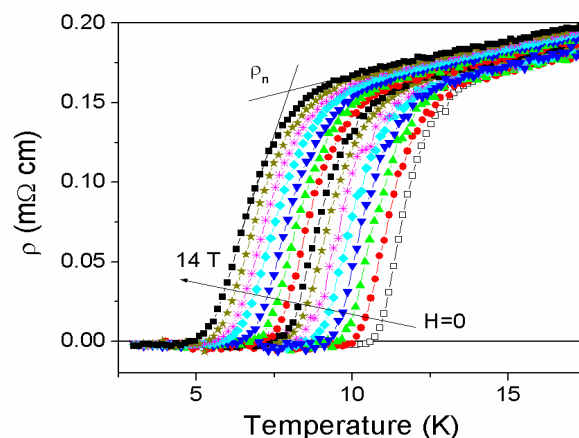


Fig. 2a. Resistivity vs. temperature dependencies at several magnetic fields.

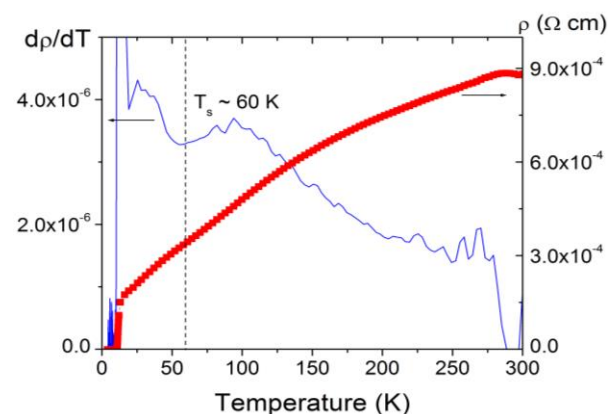


Fig. 2b. Temperature dependencies of the resistivity and its derivative at $H=0$. T_s is the temperature of a structural phase transition.

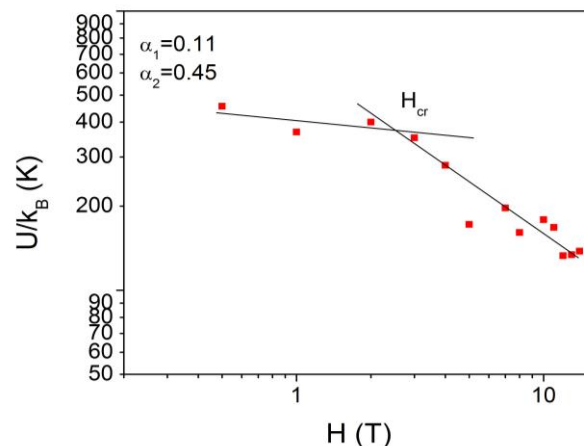


Fig. 2c. Field dependence of the activation energy in a double-logarithmic plot. The data are fitted by $U_0 \sim H^{-\alpha}$ shown as straight lines. The arrow marks the crossover from single-vortex pinning to collective pinning.

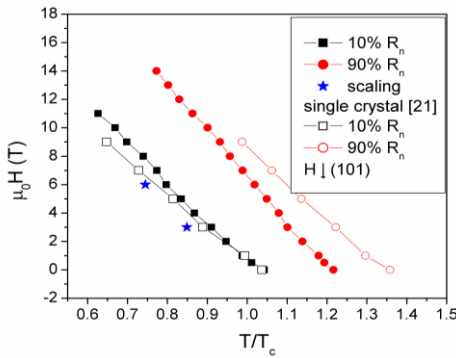


Fig. 2d. Temperature dependencies of the irreversibility line $H_{irr}(T/T_c)$ and the upper critical field $H_{c2}(T/T_c)$ determined from resistivity measurements at 10% and 90% from the normal state resistivity, respectively. Shown is also the $H_{irr}(T/T_c)$ and $H_{c2}(T/T_c)$ line for a β -FeSe single crystal [21].

Thermal fluctuation effects are another important reason for disorder effects in the mixed state. The strength of this effect is quantified by the Ginzburg number $G_i = \frac{1}{2} \left[\frac{k_B T_c}{4\pi\mu_0 H_{c2}(0) \varepsilon \xi_{ab}} \right]^2$, where ε is the anisotropy,

ξ_{ab} is the in-plane coherence lengths, k_B - Boltzmann and μ_0 - magnetic constants. Using the following relations for the thermodynamic critical field $H_c = \frac{\Phi_0}{2^{3/2} \pi \lambda_0 \xi_{ab}}$ with Φ_0

- quantum flux; the London penetration depth $\lambda_0 \sim \sqrt{\frac{m}{n}}$ with m - carrier mass and n - carrier density and $\xi_{ab} \cong \frac{\hbar v_F}{2\pi k_B T_c}$ with the Fermi velocity $v_F \sim \frac{(3\pi^2 n)^{1/3} \varepsilon^{1/6} \hbar}{m}$ the

Ginzburg number can be written as:

$$G_i \propto \varepsilon^{-4/3} m^4 T_c^4 n^{-8/3} \quad (1)$$

Obviously, along with T_c the large effective mass and low carrier density also are very important for increasing the G_i value [22]. For iron chalcogenides (Fe-11) the enhancement of G_i is a result of its low carrier density and its large effective mass $m \sim (5-16) m_0$, where m_0 is the free-electron mass [23]. Thus, thermal fluctuations are essential in cuprates ($G_i \sim 10^{-1}$ for YBCO [24]) and iron based superconductors (in particular for chalcogenides - $G_i \sim 10^{-3}$ for FeSe [24]) although in the former they are mainly a result of the high T_c , and in the latter due to their low carrier density and large effective mass.

Comparing the G_i values for FeSe and the obtained pinning force density $G_{id} = (J_c/J_0)^3$ for the investigated crystal we found that $G_{id} \ll G_i$ which ensures the observation of the vortex - glass to vortex-liquid transition [18].

Transport measurements were performed to confirm the existence of the mentioned transition in the mixed state. The current-voltage characteristics were measured in a wide temperature range (5K - 12.5K) with an interval of 0.5 K at fixed magnetic field. In **Fig. 3a** and **Fig. 4a** the ρ -J curves for different temperatures are presented at $H = 3T$ and $6T$. In both cases, a crossover from a negative curvature (at low temperatures) to a positive curvature (at higher temperatures) is observed. The negative curvature of

ρ -J isotherms is a signature of a vortex glass state [7]. At low temperatures the ρ -J isotherms almost overlap. In this case pinning barriers are high enough and almost prevent thermal fluctuations, which results in very small changes in the current. With increasing temperature, the distance between the ρ -J curves grows and the curvature of isotherms falls down until it disappears completely. Each ρ -J curve (in double logarithmic scale) was fitted by a quadratic polynomial function starting from low temperatures. The absolute value of the coefficient in the quadratic term decreases with increasing temperature until it reaches zero. The lowest temperature at which the quadratic term disappears and the ρ -J curve is linearly fitted is denoted as T_g . This procedure is used to determine T_g values at $H=3T$ and $H=6T$. Going back to **Fig. 2d** it is important to mention that the two blue star points ($T_g=9.0K$, $H=3T$) and ($T_g=8.0K$, $H=6T$) determined from this fitting procedure are part of the line below which a vortex-glass state with zero resistance is realized. The $H_{irr}(T/T_c)$ line obtained from $\rho(T)$ curves at different magnetic fields using the $0.1\rho_n$ criterion is lightly shifted to higher fields and temperatures in comparison to (T_g , H) blue points. This indicates that the T_g value is properly determined in the frame of the given error (maximum error for T_g is estimated by the step size in T). At temperatures above T_g a positive curvature characterizing ρ -J isotherms, reflects the vortex liquid state and especially the TAFF regime [7]. A further increase of the temperature establishes the flux flow regime with ρ -J isotherms directed parallel to the x axis.

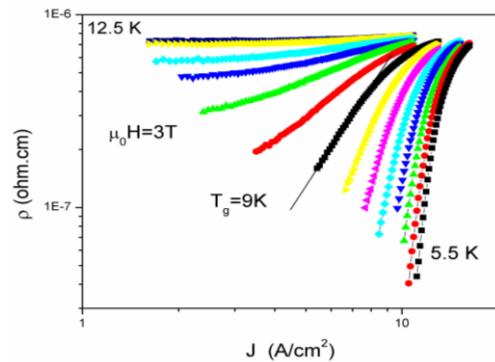


Fig. 3a. $\rho(J)$ curves at several temperatures and $H=3T$. The VG-VL transition temperature, T_g is marked.

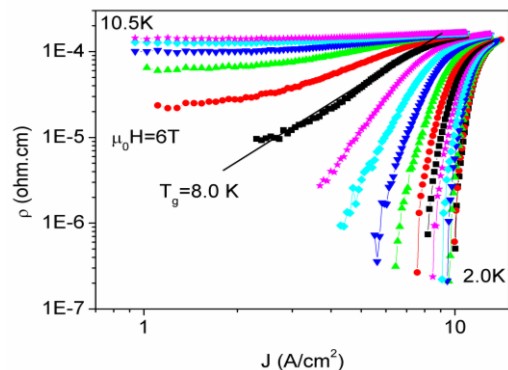


Fig. 4a $\rho(J)$ curves at several temperatures and $H=6T$. The VG-VL transition temperature, T_g is marked.

According to the VG theory [5] the existence of a continuous phase transition in the vortex matter can be proved by the collapse of E-J characteristics in two master curves from both side of T_g after scaling. At this phase transition a power law divergence for the correlation length $\xi_g \sim |T-T_g|^{-\nu}$ and relaxation time $\tau \sim \xi_g^z \sim |T-T_g|^{-\nu z}$ is expected, where z and ν are dynamic and static scaling exponents, respectively. The vortex correlation length ξ_g represents the topological difference between fluctuating vortices in the VG state and their equilibrium configuration, while τ is the time needed for vortex relaxation [4]. According to [7] ξ_g can be estimated by using the relation:

$$J_c = \frac{k_B T}{\phi_0 \xi_g^{(D-1)}}, \quad (2)$$

where J_c is the critical current density at $T < T_g$ and D is the vortex dimensionality. At $H=3$ T and $T=2$ K the critical current density was determined to be $J_c = 2.4 \cdot 10^3$ A/cm² [19] and the estimated value for the vortex correlation length is $\xi_g = 23.6$ nm. This value of ξ_g is large enough compared with the lattice parameter c of the unit cell of the superconducting tetragonal phase ($c=5.514$ Å), confirming the 3D vortex dimensionality. At these conditions ($H=3$ T and $T=2$ K) the intervortex spacing $a \sim (\Phi_0/B)^{1/2}$ is approximately 26.2 nm and $\xi_g < a$ as it should be in the VG state. For increasing temperature, the critical current decreases and ξ_g increases. At temperatures $T > T_g$ as a result of a larger correlation length the opposite relation ($\xi_g > a$) is valid in the VL state.

For the scaling procedure, the universal scaling function is used: $Y=(E/J)|1-T/T_g|^{(D-z-2)}$ versus $X=(J/T)|1-T/T_g|^{(1-D)}$. A precise determination of the scaling exponents is needed for a successful scaling. The predicted power law dependence for $\rho(J)$ at $T=T_g$: [5]

$$\rho(J, T=T_g) \sim J^{(z-1)/(D-1)} \quad (3)$$

was used for the determination of z .

The dependence (3) presented in double logarithmic scale is a straight line and its slope is equal to $(z-1)/(D-1)$. From $\log(\rho)$ vs $\log(J)$ curves at $T=T_g=9.0$ K (for $H=3$ T) and $T_g=8.0$ K (for $H=6$ T) the slope of the lines was found (Fig. 3a and Fig. 4a). Assuming 3D dimensionality the following values were determined for the dynamic exponents: $z=5.84 \pm 0.02$ ($H=3$ T) and $z=5.40 \pm 0.01$ ($H=6$ T). The static exponent ν was determined from the resistivity vs temperature dependence (at $H=3$ T and $H=6$ T) at low current. In the vortex liquid state, $T > T_g$ the linear resistivity at low current is given by: [2]

$$\rho_{lin} \propto (T - T_g)^{\nu(z+2-D)} \quad (4)$$

This dependence in double logarithmic scale is presented in Fig. 3b and Fig. 4b for $H = 3$ T and $H = 6$ T, respectively. From the slope of the linear part in these figures the following values for the static exponents are determined: $\nu = 0.26 \pm 0.02$ for $H = 3$ T and $\nu = 0.30 \pm 0.02$ for $H = 6$ T.

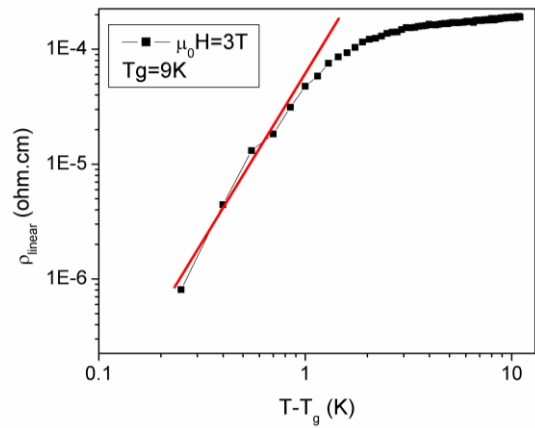


Fig. 3b. Double logarithmic plot of linear resistivity vs. $(T-T_g)$ at $H=3$ T. The red line is a linear fit to the data.

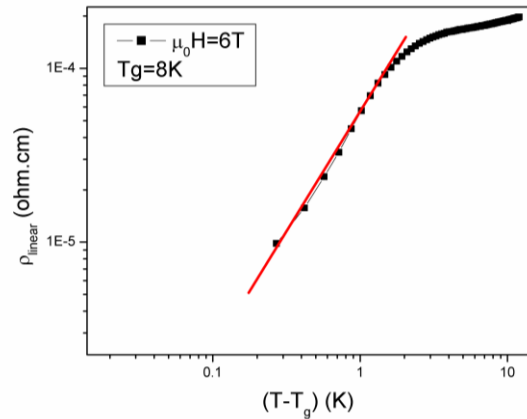


Fig. 4b. Double logarithmic plot of linear resistivity vs. $(T-T_g)$ at $H=6$ T. The red line is a linear fit to the data.

According to the vortex glass model [2] the scaling exponents should be field independent and their values should be $z \approx 4-7$ and $\nu \approx 1-2$, respectively. Similar values are obtained for the investigated $Fe_{1.02}Se$ crystal in the field range between 3 T and 6 T. For the z exponent these values belong to the predicted interval, while for ν exponent a little bit smaller values are obtained than those predicted by the model. This is a result from the type of disorder and normal state resistivity [25] in the crystal. The investigated $Fe_{1.02}Se$ sample has a complex morphology described as an aggregate of domains. It's $J_c(T)$ dependence is quadratic and characteristic for a SNS (superconductor-normal metal-superconductor) path of the current through the sample [19]. In this context, the crystal might possess a similar granularity as polycrystalline samples reflecting the resistivity and static exponent respectively.

In Fig. 5a and Fig. 5b the scaling collapse at $H=3$ T and $H=6$ T is presented respectively, analogously to what found in other iron based superconductors: $NdFeAsO_{0.85}$, [26] $BaFe_2As_2$, [25] $(Ba, K) Fe_2As_2$, [27] $BaFe_{1.8}Co_{0.2}As_2$, [28] $FeSe_{1-x}Te_x$, [29] $Fe_{1.01}Te_{0.62}Se_{0.38}$ [30]. This confirms the existence of a second order phase transition in the vortex matter in $Fe_{1.02}Se$ crystals similar to HTSC materials, and underlines the universality of vortex-glass to vortex-liquid transition.

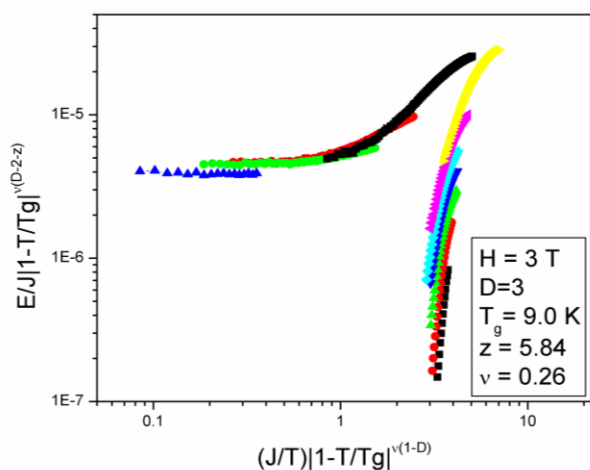


Fig. 5a. Scaling plot of the E-J data measured at $H=3T$. The corresponding scaling functions are indicated at both axis and the values of scaling parameters are given.

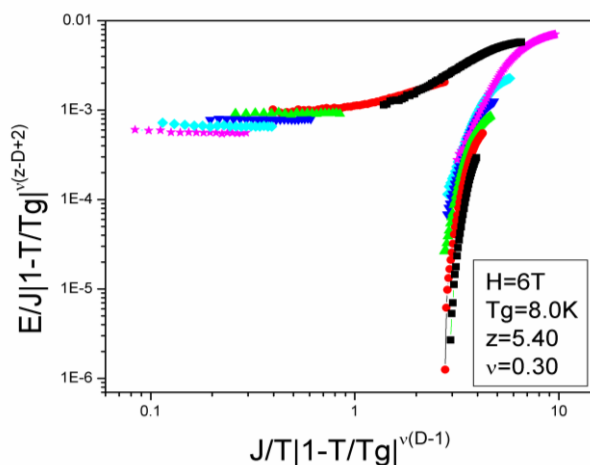


Fig. 5b. Scaling plot of the E-J data measured at $H=6T$. The corresponding scaling functions are indicated at both axis and the values of scaling parameters are given.

Conclusion

The investigated $\text{Fe}_{1.02}\text{Se}$ crystal contains nano-sized non-superconducting inclusions of a hexagonal impurity phase. These inclusions act as effective pinning centers and shift the $H_{\text{irr}}(T)$ line to higher fields and temperatures in comparison to the $H_{\text{irr}}(T)$ line of a single-phase single FeSe crystal. In spite of the low T_c of the investigated compound, thermal fluctuations are significant because of its large effective mass and its low carrier density. The interplay of pinning and thermal fluctuations results in a vortex-glass phase evidenced by the negative curvature of ρ -J isotherms at $T < T_g$ and a vortex-liquid phase with a positive curvature of ρ -J isotherms at $T > T_g$. Using the universal scaling function of the VG model, the E-J dependencies are scaled in the two master curves for both states, thus confirming the VG-VL phase transition. The determined critical exponents are practically field independent with the z values in the model predicted interval and v values a little bit smaller than the predicted by the model.

Acknowledgments

This work has been carried out within the framework of the inter-academic Italian-Bulgarian research project (Department of Physics 'E R Caianiello' CNR-SPIN unit, University of Salerno and the Institute of Solid State Physics 'Georgi Nadjakov', Bulgarian Academy of Sciences).

References

- Hirsch, J. E.; Maple, M. B.; Marsiglio, F.; *Physica C*, **2015**, *514*, 1.
- Fisher, D.; Fisher, M.; Huse, D.; *Phys Rev B*, **1991**, *43*, 130.
- Dorsey A. T.; Huang M.; Fisher M. P. A.; *Phys. Rev. B.*, **1992**, *45*, 523.
- Yeh, N. C.; Jiang, W.; Reed, D. S.; Kriplani, U.; Konczykowski, M.; Tombrello, T. A.; Holtzberg, F.; Tsuei, C. C.; *Ferroelectrics*, **1996**, *177*, 143.
- Huse, D.; Fisher, M.; Fisher, D.; *Nature*, **1992**, *358*, 553.
- Fisher, M.; *Phys. Rev. Lett.*, **1989**, *62*, 1415.
- Koch, R.; Foglietti, V.; Gallagher, W.; Koren, G.; Gupta, A.; Fisher, M.; *Phys. Rev. Lett.*, **1989**, *63*, 1511.
- Buchkov, K.; Polichetti, M.; Nenkov, K.; Nazarova, E.; Mancusi, D.; Balchev, N.; Kovacheva, D.; Zahariev, A.; Pace, S.; *Supercond. Sci. Technol.*, **2015**, *28*, 035009.
- Yuan, Z.; Lu, H.; Lio, Y.; Wang, J.; Jia, S.; *Phys. Rev. B*, **2016**, *93*, 184405.
- Sun, Y.; Pyon, S.; Tamegai, T.; *Phys. Rev. B*, **2016**, *93*, 104502.
- Johnston D.C.; *Advances in Physics*, **2010**, *59*, 803.
- Liu, X.; Zhao, L.; He, S.; He, J.; Liu, D.; Mou, D.; Shen, B.; Hu, Y.; Huang, J.; Zhou, X.; *J. Phys. Condens. Matter.*, **2015**, *27*, 183201.
- Watson, M. D.; Kim, T. K.; Haghighirad, A. A.; Davies, N. R.; McCollam, A.; Narayanan, A.; Blake, S. F.; Chen, Y. L.; Ghannadzadeh, S.; Schofield, A. J.; Hoesch, M.; Meingast, C.; Wolf, T.; Coldea, A. I.; *Phys. Rev. B*, **2015**, *91*, 155106.
- Watson, M. D.; Yamashita, T.; Kasahara, S.; Knafo, W.; Nardone, M.; Beard, J.; Hardy, F.; McCollam, A.; Narayanan, A.; Blake, S. F.; Wolf, T.; Haghighirad, A. A.; Meingast, C.; Schofield, A. J.; Löhneysen, H.; Matsuda, Y.; Coldea, A. I.; Shibauchi, T.; *Phys. Rev. Lett.*, **2015**, *115*, 0270006.
- Anderson, P. W.; *Phys. Rev. Lett.*, **1962**, *9*, 39.
- Anderson, P. W.; Kim, Y. V.; *Rev. Mod. Phys.*, **1964**, *36*, 39.
- Leo, A.; Grimaldi, G.; Guarino, A.; Avitabile, F.; Nigro, A.; Galluzzi, A.; Mancusi, D.; Polichetti, M.; Pace, S.; Buchkov, K.; Nazarova, E.; Kawale, S.; Bellingeri, E.; Ferdeghini, C.; *Supercond. Sci Technol.*, **2015**, *28*, 125001.
- Blatter, G.; Feigel'man, M. V.; Geshkenbein, V. B.; Larkin, A. I.; Vinokur, V. M.; *Rev. Mod. Phys.*, **1994**, *66*, 1125.
- Galluzzi, A.; Polichetti, M.; Buchkov, K.; Nazarova, E.; Mancusi, D.; Pace, S.; *Supercond. Sci Technol.*, **2015**, *28*, 115005.
- Nazarova, E.; Balchev, N.; Nenkov, K.; Buchkov, K.; Kovacheva, D.; Zahariev, A.; Fuchs, G.; *Supercond. Sci. Technol.*, **2015**, *28*, 025012.
- Lei, H.; Hu, R.; Petrovich, C.; *Phys. Rev. B*, **2011**, *84*, 014520.
- Gurevich, A.; *Rep. Prog. Phys.*, **2011**, *74*, 124501.
- Tamai, A.; Ganin, A.Y.; Rozbicki, E.; Bacsca, J.; Meevasana, W.; King, P. D. C.; Caffio, M.; Schaub, R.; Margadona, S.; Prassides, K.; Rosseinsky, M. J.; Baumberger, F.; *Phys. Rev. Lett.* **2010**, *104*, 097002.
- Yang, H.; Chen, G.; Zhu, X.; Xing, J.; Wen, H. H.; *Phys. Rev. B*, **2017**, *96*, 064501.
- Ghorbani, S. R.; Wang, X. L.; Shabazi, M.; Dou, S. X.; Choi, K. Y.; Lin, C. T.; *Appl. Phys. Lett.*, **2012**, *100*, 072603.
- Liu, Y.; Chai, Y. S.; Kim, H. J.; Stewart, G. R.; Kim, K. H.; *J. Korean Phys. Soc.*, **2009**, *55*, L383.
- Kim, H. J.; Liu, Y.; Oh, Y. S.; Khim, S.; Kim, I.; Stewart, G. R.; Kim, K. H.; *Phys. Rev. B*, **2009**, *79*, 014514.
- Choi, K. Y.; Kim, K. H.; *Prog. Supercond. & Cryog.*, **2013**, *15*, 16.
- Chang, H. H.; Luo, J. Y.; Wu, C. T.; Hsu, F. C.; Huang, T. W.; Wu, P. M.; Wu, M. K.; Wang, M. J.; *Supercond. Sci. Technol.*, **2011**, *24*, 105011.
- Yu, Y.; Wang, C.; Li, Q.; Wang, H.; Zhang, C.; *J. Phys. Soc. Jpn.*, **2014**, *83*, 114701.